Prostate Cancer Diagnosis and Staging

Aradhana M. Venkatesan[1]

Prostate cancer is the most common cancer and second leading cause of cancer death in American men. Imaging plays a central role in the diagnosis and staging of prostate cancer, which makes the role of the radiologist critical to the multidisciplinary management of patients with prostate cancer. This necessitates a working knowledge of prostate anatomy, histologic grading and clinical staging, and the role and utility of specific imaging modalities for detection and staging.

Prostate cancer is the most common cancer in American men, with approximately one in nine men diagnosed with prostate cancer during his lifetime. The 2018 American Cancer Society estimates there are 164,000 new cases of prostate cancer to be diagnosed in 2018 and nearly 30,000 deaths. Although most men diagnosed with prostate cancer do not die of it, prostate cancer remains the second leading cause of cancer death [1]. The Gleason score is assigned to prostate histologic specimens on the architectural appearance of tumor and is defined as the sum of the two most commonly observed grade patterns in a histologic specimen, with combined pathologic scores ranging from 2 to 10, and with a higher number indicating greater risks and higher mortality [2]. Together with the prostate-specific antigen (PSA) and tumor stage, Gleason score is incorporated into a strategy of prostate cancer staging that predicts prognosis and helps guide therapy [3]. The use of serum PSA as a screening tool was adopted in the early 1990s, resulting in a dramatic increase in the incidence of prostate cancer. Most of these cancers were clinically localized and associated with an increase in aggressive treatments (radical prostatectomy and radiation therapy) for early stage disease [4]. At present, prostate cancer is typically diagnosed in the setting of a suspicious serum PSA concentration or digital rectal examination [2]. The primary goal during baseline evaluation is to establish disease presence and extent. Diagnosis is possible via transrectal ultrasound (TRUS)–guided biopsy, ultrasound (US)/MRI fusion-guided biopsy, or MRI-targeted biopsy. Increasingly, initial staging and diagnosis is done with multiparametric MRI (mpMRI) and MRI directed biopsies. The Prostate Imaging and Reporting and Data System version 2 (PI-RADSv2) provides a structured schema for global standardization in the acquisition, interpretation, and reporting of prostate mpMRI examinations. PI-RADSv2 was published by a steering committee comprising the joint efforts of the American College of Radiology (ACR), European Society of Urogenital Radiology (ESUR), and AdMeTech Foundation [5]. Recent data describing mpMRI- and MRI-directed biopsies using PI-RADSv2 suggest use of this system improves the detection of clinically significant prostate cancers likely to cause harm and at the same time decreases the detection of clinically insignificant cancers. To ensure the quality of the diagnostic process, the joint working of radiologists and urologists, conducting biopsy procedures within multidisciplinary teams, is encouraged [6]. In patients for whom pretreatment imaging and biopsy confirm the presence of intermediate- or high-risk disease, bone scintigraphy and CT are primarily used to detect bone and nodal metastases [2]. There are increasing data employing PET/CT and, more recently, PET/MRI performed with prostate cancer-specific radiotracers, such as ^{11}C and ^{18}F choline, ^{18}F fluciclovine, ^{68}Ga, and ^{18}F prostate-specific membrane antigen (PSMA) for recurrence detection, particularly in the low PSA setting, with data, to a lesser extent, on the role of these agents for primary tumor detection and staging. Although discussion of these study findings is beyond the scope of this chapter, these data are anticipated to contribute to the management of prostate cancer patients in the future. PET/CT and PET/MRI performed with tracers such as ^{11}C choline and ^{68}Ga prostate-specific membrane antigen have the potential to improve detection, staging, and recurrence detection in the low-PSA setting and remain under study in the context of clinical trials; review of these emerging data is beyond the scope of this chapter.

Prostate Anatomy

A fundamental understanding of normal prostate anatomy is essential to diagnostic accuracy. In the coronal plane, the prostate gland can be subdivided into the base (the upper one-third of the prostate just below the urinary bladder), the mid gland (the middle one-third of the prostate that includes the verumontanum in the mid prostatic urethra), and apex (the lower one-third of the prostate) [7]. These anatomic descriptors are pertinent to lesion

Disclosures: Dr. Venkatesan has received grant support from the Radiological Society of North America, Toshiba America Medical Systems, and The University of Texas MD Anderson Cancer Center.

[1]Department of Diagnostic Radiology, Section of Abdominal Imaging, The University of Texas MD Anderson Cancer Center, 1400 Pressler St, FCT 15.6074, MSC 1182, Houston, TX 77030. Address correspondence to A. M. Venkatesan (avenkatesan@mdanderson.org).

localization on transrectal US, US-guided biopsy, and MRI.

In the axial plane, the prostate can be divided into three zones apparent on mpMRI but typically poorly delineated or inapparent on TRUS or CT. These zones include the outer peripheral zone, containing approximately 70% of all glandular tissue, which is typically hyperintense in signal on T2-weighted imaging. The periurethral transition zone, containing 5% of all glandular tissue, is typically heterogeneous in signal on T2-weighted imaging, particularly in the setting of benign prostatic hypertrophy (BPH). The central zone, comprising 20% of all glandular tissue, typically appears as a bandlike T2 hypointense structure located between the periurethral transition zone and outer peripheral zone, extending from below the ejaculatory ducts to the verumontanum [8]. The anterior fibromuscular stroma, a continuation of the capsular gland margin anteriorly, is devoid of glandular tissue. It appears as a crescentic band of low signal on both T1- and T2-weighted imaging that is relatively hypovascular on dynamic contrast-enhanced (DCE) images [8, 9]. Because most prostate cancers arise from glandular tissue, knowledge of the distribution of glandular tissue by anatomic location is pertinent [8–11]. It is also important to note that the peripheral zone varies from base to apex, with the transition zone dominating at the level of the bladder neck and prostate base, whereas peripheral zone comprises most of the prostatic apex [8–11].

At the periphery of the transition zone in the axial plane, the surgical capsule comprises a thin rim of tissue, typically compressed in the setting of BPH. It can be appreciated on axial T2-weighted MRI as a bandlike crescentic area of reduced signal on T2-weighted imaging and serves as one of the anatomic landmarks to urologists during transurethral resection of the prostate for BPH [12]. It is distinct from the anatomic (pseudo)capsule, located along the outer aspect of the peripheral zone, which serves as an important landmark for local tumor staging because tumor extracapsular extension upstages a patient and typically indicates a poorer prognosis [10].

Important periprostatic structures include the seminal vesicles, neurovascular bundles, the bladder neck, external urethral sphincter, and penile bulb. The seminal vesicles appear as saccular cystic structures that are anechoic on US, hypodense on CT, and hyperintense on T2-weighted MRI. They are located above the base of prostate, join the ejaculatory ducts at the prostate base, and drain into the prostatic urethra through the verumontanum [9, 10]. They are best evaluated on both axial and coronal T2-weighted images, particularly when screening for seminal vesicle tumor involvement [9].

Important periprostatic structures include the bladder neck, external urethral sphincter, and neurovascular bundles. Similar to the delineation of prostate subglandular anatomy, these structures are best delineated on mpMRI as compared with US or CT. Located either within or adjacent to the prostate base is the bladder neck. In some patients, a distinct bladder neck can be seen on coronal T2-weighted MRI, located superior to the prostate base. As the prostate enlarges, it expands, with obliteration of the bladder neck by the central gland, which typically projects into the bladder lumen [9]. Adjacent and usually below the prostate apex, the external sphincter is visualized by mpMRI. The external sphincter contains both the membranous urethral sphincter, surrounding the urethra between the prostate apex and penile bulb and the intraprostatic sphincter that surrounds the urethra from the verumontanum to the prostate apex [9]. The neurovascular bundles are typically seen on mpMRI as discrete rounded structures on T2-weighted imaging and apparent diffusion coefficient (ADC) imaging in the 5 and 7 o'clock positions relative to the gland in the axial plane. The periprostatic venous plexus can be observed along the lateral margins of the peripheral zone as areas of relative signal void [9]. It should be noted, however, as per prior studies, that significant variability in neurovascular bundle location and distribution around the prostate gland is possible [13]. Moreover but rarely, no neurovascular elements may be apparent on imaging [9, 13].

The PI-RADSv2 structured reporting schema uses a detailed anatomic sector map. It uses 39 sectors or regions, which the reader is encouraged to review [5]. The sector map is meant to enable radiologists, urologists, pathologists, and others to localize findings described in MRI reports and to serve as a visual aid for discussions with patients [5].

Overview of Imaging Modalities for Detection and Staging

As summarized in the most recent ACR Appropriateness Criteria for the Pretreatment Detection, Surveillance, and Staging of Prostate Cancer, the common modalities used to evaluate prostate cancer are TRUS, MRI, CT, and bone scintigraphy [3]. At present, TRUS and MRI are used to diagnose and stage local disease extent, whereas CT and bone scintigraphy are used to evaluate for metastatic disease, which typically involves either lymph nodes or osseous structures [3].

An increased likelihood of locally advanced or distant disease has been observed in patients with intermediate- and high-risk disease, underscoring the importance of risk stratification [3]. The National Comprehensive Cancer Network (NCCN) criteria for high-risk disease include a PSA of 20 ng/mL or more, Gleason score higher than 8, clinical stage T3 or higher or any two of the following: T2b or T2c clinical stage, Gleason score of 7 or more, PSA of 10–20 ng/mL [14].

Transrectal Ultrasound and Transrectal Ultrasound–Guided Biopsy

The role of TRUS is primarily for the localization of the prostate gland before systematic biopsy [3] and is typically performed by urologists or, in some instances, by interventional radiologists. A minority of prostate cancers are apparent on US, and it has limited value for tumor detection and local staging. Despite significant concerns related to both underdiagnosis and overdiagnosis, TRUS-guided systematic prostate biopsy remains the standard of care for diagnosis in patients with clinically suspected prostate cancer [3].

Multiparametric MRI

Multiparametric MRI reflects a combination of anatomic T1- and T2-weighted sequences and functional MR-imaging sequences (DWI and DCE). Historically, given the standard use of TRUS-guided systematic biopsy for prostate cancer diagnosis, MRI has not been widely used in biopsy-naïve patients with clinically suspected prostate cancer on the basis of an abnormal digital rectal examination or serum PSA concentration [3]. However, the superior spatial resolution of mpMRI as compared with US and CT for the assessment of the prostate and periprostatic anatomy and the emerging literature on the use of MRI targeting to guide baseline prostate biopsy support routine use of MRI for tumor localization [3, 15]. The reader is encouraged to review references describing the advantages of endorectal coil (ERC) use for dedicated prostate mpMRI use [16–20]. As described in PI-RADSv2, for some 1.5-T MRI systems, particularly older ones, use of an ERC is considered indispensable to achieve diagnostic high-resolution imaging of the prostate [5]. At the same time, previous studies suggest that 3-T field strength without an ERC may offer sufficient image quality to identify clinically significant prostate cancers [21, 22], although direct comparison of both strategies for cancer detection or staging is lacking. Taking these factors and the variability of MRI equipment available in clinical use into consideration, the PI-RADS Steering Committee recommends that supervising radiologists strive to optimize imaging protocols to obtain the best and most consistent image quality possible with the MRI scanner used, while bearing in mind cost, availability, and patient preference [5].

Prostate cancers typically present as foci of hypointense signal on T2-weighted imaging, associated with restricted diffusion, i.e., increased signal on DWI and corresponding reduced signal on ADC maps. Prostate cancers in the peripheral zone typically stand out as foci of reduced signal on T2-weighted imaging, relative to the normal surrounding glandular tissue that is hyperintense on T2-weighted imaging (Fig. 1). Transition zone cancer foci are more challenging to identify on T2-weighted images owing to the heterogeneous appearance of the transition zone, which can contain stromal benign prostatic hypertrophy (BPH) nodules, both of which are hypointense on T2-weighted imaging and can mimic the appearance of cancer [10]. There is known overlap in the quantitative T2 signal intensity, ADC values, and DCE K_{trans} values between stromal BPH nodules and transition zone cancers [23, 24]. To detect transition zone cancers, scrutiny of the margins of a lesion can be helpful because transition zone cancer foci typically have poorly defined margins, which have been described as having a smudged or erased charcoal appearance [10] (Fig. 2). Irrespective of their site within the prostate, high-grade cancers tend to have lower signal intensity than low-grade cancers and will generally appear lower in signal on T2-weighted images relative to the surrounding prostate parenchyma [10, 25]. T2-weighted MRI has a reported range in sensitivity of 27–100% and specificity of 32–99% for cancer detection [10, 26–28]. Alongside assessment of the T2-weighted images, it is important to review the T1-weighted images to identify the presence of postbiopsy hemorrhage. These appear as foci of increased signal on T1-weighted images, most often within the peripheral zone or within lumen of the seminal vesicles [10]. Hemorrhagic foci with increased signal on T1-weighted images will show corresponding reduced signal on T2-weighted images, which should not be confused with cancer. Cross correlation of the T1-weighted and T2-weighted images is crucial to avoid this pitfall.

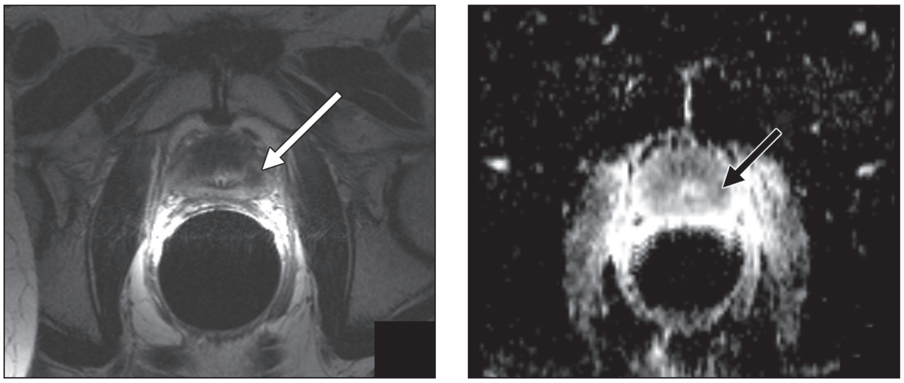

A B

Fig. 1—72-year-old man with biopsy-confirmed Gleason 9 cancer of left prostatic apex.
A, Axial T2-weighted MRI of prostate shows focus of reduced T2 signal in left prostatic apex (*arrow*).
B, Corresponding apparent diffusion coefficient map shows reduced signal corresponding to signal abnormality on T2-weighted images (*arrow*).

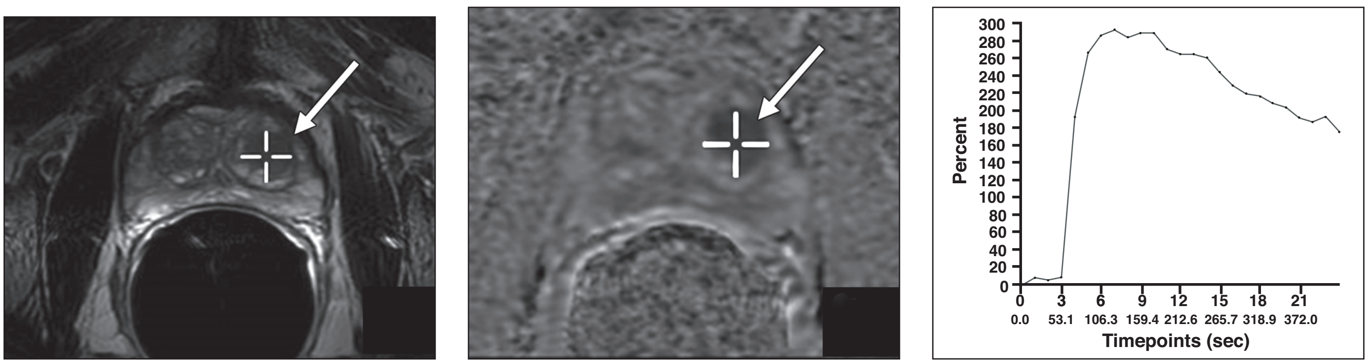

A B C

Fig. 2—70-year-old man with biopsy-confirmed Gleason 8 prostate cancer involving left transition zone.
A, Axial T2-weighted MRI of prostate shows lentiform focus of reduced T2 signal in left transition zone (*arrow,* +).
B, Corresponding apparent diffusion coefficient map show reduced signal corresponding to signal abnormality on T2-weighted images (*arrow,* +).
C, Contrast enhancement time curve at level of abnormal focus shows type 3 (washout) curve appearance most commonly associated with malignancy.

On DWI, prostate cancers show restricted diffusion manifest as increased signal on DWI and corresponding low-signal intensity on ADC maps [10]. When used in conjunction with T2-weighted image, DWI and ADC maps increase the sensitivity for prostate cancer detection (54–98%) [10, 26, 29]. Using a high b value for DWI is helpful to distinguish prostate cancer from normal prostatic parenchyma and prostatitis [10]. Per PIRADSv2, DWI should include an ADC map and high b-value images, defined as a b-value greater than or equal to 1400 s/mm^2 [5]. DWI is also useful to assess tumor aggressivity, with prior work having shown that tumors with high Gleason scores exhibit lower ADC values than lower Gleason grade tumors [30, 31].

DCE-MRI serves as a complementary tool alongside DWI and T2-weighted images, with prior studies describing a specificity of 93.8% and positive predictive value of 94.7% [32]. DCE images can be evaluated qualitatively and quantitatively. Qualitative assessment involves the assessment of contrast enhancement time curves at the level of tumor as compared with the normal parenchyma. The appearance of the time–signal intensity curves has been subdivided into progressive (type 1), plateau (type 2), or washout (type 3). The washout curve, showing a drop-off in signal intensity with time after a rapid initial rise in the beginning, is considered the most suspicious for prostate cancer, especially if there is a focal asymmetric enhancing lesion, although type 1 and 2 curves can be observed for prostate cancers as well [33]. Quantitative assessment uses a pharmacokinetic model that, after software-based postprocessing, may be displayed as color-coded maps. Regions of the prostate that are low in T2 signal and show corresponding rapid wash-in and washout or high K_{trans} or K_{ep} relative to the normal prostatic parenchyma are more suspicious for cancer [10]. The high specificity of DWI and DCE-MRI can help to enhance diagnostic accuracy and reduce the number of lesions targeted when MRI is used in the setting of prostate biopsy [10, 34].

MRI-Targeted Biopsy

TRUS or MRI may be combined with biopsy. MRI-targeted biopsy can be performed via direct or in-bore sampling, via US/MRI fusion, or with cognitive fusion. With the direct or in-bore approach, real-time MRI guidance is used for lesion-directed biopsy. With US/MRI fusion, the patient undergoes a standard TRUS-guided biopsy, with MRI targets selected from a preacquired MRI scan whose data are coregistered to the intraprocedural US images via common anatomic landmarks; additional cores are taken from the areas of suspicion delineated on MRI [3]. With cognitive fusion, the patient undergoes a standard TRUS-guided biopsy, but the operator also biopsies the MRI target on the basis of visual anatomic coregistration and freehand needle insertion. Several studies [35–37] have illustrated the inferiority of cognitive fusion as compared with US/MRI fusion [3]. In contrast, advantages for both targeted MR/US fusion-guided prostate biopsy and direct MRI-targeted biopsy over standard sextant US-guided biopsy have been shown [38, 39]. In a prospective cohort study of 1003 men undergoing both targeted and standard biopsy referred for elevated PSA or abnormal digital rectal examination results, targeted MRI/US fusion biopsy, compared with standard extended-sextant US-guided biopsy, showed increased detection of high-risk prostate cancer and decreased detection of low-risk prostate cancer [38]. A prior meta-analysis found that MRI-targeted biopsy significantly increased the detection rate for all cancers and significantly decreased the detection of clinically insignificant cancers [39]. These and similar data are anticipated to change current approach to prostate cancer diagnosis in the future, which has historically involved a TRUS-guided sextant biopsy before or in the absence of dedicated prostate imaging [3]. At present, MRI-guided biopsy may be used for baseline diagnosis in patients who have had a negative TRUS-guided biopsy and elevated PSA or other cause for clinical concern, for reevaluation of tumor grade in patients on active surveillance, and for diagnosis of local recurrence [3]. Experience with MRI-targeted biopsy suggests that this approach is associated with fewer false negatives, better tumor characterization, improved tumor localization, and better treatment stratification as compared with traditional systematic biopsy, particularly for lower-risk cohorts that may be appropriate for active surveillance or focal therapy [38–43]. It is anticipated that MRI-targeted biopsy will supplant TRUS-guided sextant biopsy as the clinical standard for prostate cancer diagnosis in the future [3].

CT

The primary role of CT in prostate cancer is the detection of nodal metastases. On occasion, the primary tumor can be seen as an area of focal enhancement within the prostate on contrast-enhanced CT [3]. A prior meta-analysis has showed a pooled sensitivity of 0.42 (95% CI, 0.26–0.56) and specificity was 0.82 (95% CI, 0.8–0.83) [44]. Similar findings have been shown in other prior studies [45]. These results likely reflect limitations of the assumption that nodal size reflects nodal histologic composition; it is known that this assumption has limited accuracy [3]. The NCCN guidelines recommend CT if clinical stage is T3 or T4 or if a nomogram-based probability of lymph node involvement exceeds 10% [14].

Bone Scan

Technetium-99m-methyl diphosphonate (^{99m}Tc-MDP) radionuclide bone scan remains the standard test used for detection of bone metastases in high-risk patients. There are data to suggest that emerging techniques like PET/CT with radiotracers such as sodium fluoride, prostate cancer specific radiotracers such as ^{11}C and ^{18}F choline, ^{18}F fluciclovine, and ^{68}Ga, and ^{18}F PSMA, or possibly whole-body MRI may replace the traditional bone scan in the future [3]. In the absence of these techniques, it is preferable for bone scintigraphy to be performed with SPECT/CT capability to maximize anatomic localization of suspected metastatic foci [3]. Meta-analysis data have described a sensitivity of 0.79 (95% CI, 0.73–0.83) and specificity of 0.82 (95% CI, 0.78–0.85) for the diagnosis of bone metastases by bone scintigraphy [46]. NCCN guidelines [14] recommend bone scintigraphy if baseline PSA is 20 or more, clinical stage is T2 and PSA is 10 or higher, clinical stage is T3 or T4, Gleason score is 8 or more, or any symptoms are suggestive of osseous metastatic involvement [3].

Clinical Staging of Prostate Cancer

Staging of prostate cancer is based on local, nodal, and distant disease extent [10, 47, 48]. Once a focal lesion consistent with prostate cancer is detected, e.g., on mpMRI, there is the opportunity to determine the degree of locoregional tumor extent. The most important overall assessment is whether the tumor is confined to the gland (T stage ≤ 2) or extends beyond the prostate gland (≥ T3). When the capsular margin or anterior fibromuscular stroma is involved by a focus of cancer, it is reported as capsular invasion. When the cancer focus extends into the periprostatic adipose and vascular or venous tissue, it is interpreted as extraglandular or extracapsular extension, consistent with T3a disease [10, 47, 48]. A characteristic pattern of spread involves the obliteration of the normally T2-hyperintense wedge shape of the rectoprostatic angle seen on axial T2-weighted images by posteriorly located prostate cancers. Seminal vesicle invasion (SVI) indicates T3b disease and typically occurs at the prostate base by direct extension across the base into the inferior seminal vesicles [13]. Signs of SVI include seminal vesicle wall thickening or replacement of the normal seminal vesicles by cancer [10]. T4 disease includes tumor involvement of the muscular wall of the bladder or rectum or tumor extension to the pelvic side wall or levator muscles [10, 47, 48].

Nodal staging involves detection of metastasis in regional nodal stations, including the external iliac, internal iliac, and obturator nodes. Prior studies have suggested an association between the number of nodes involved and prognosis, with one to two positive nodes associated with a recurrence-free survival of 70% and with more than five positive nodes associated with a recurrence-free survival of 49% [10, 49]. Nodal staging with MRI relies primarily on size to determine the level of suspicion for metastatic involvement. Size criteria have limitations given the significant overlap with nonmalignant nodes, with specificity decreased when sensitivity is maximized and vice versa [10]. In general, nodes measuring greater than 0.8 cm in short axis in the internal iliac, external iliac, and obturator stations are considered enlarged and suspicious for metastatic involvement. Common iliac nodes larger than 0.8 cm and retroperitoneal nodes greater than 1.0 cm in short axis are generally considered suspicious for metastatic disease [10]. For normal vs suspicious nodes in the perirectal region, 5-mm short-axis diameter nodes may be considered the cutoff [10, 50]. Shape and internal signal intensity can be useful in nodal assessment. A node that is round (instead of ovoid) or irregular in contour is more likely to be metastatic. Heterogeneous signal intensity on T2-weighted MRI is observed for prostate cancer nodal metastases as demonstrated for other cancer histologies [10, 51, 52].

Distant metastases include nonregional nodes and osseous metastases. On prostate MRIs, these areas can be evaluated on

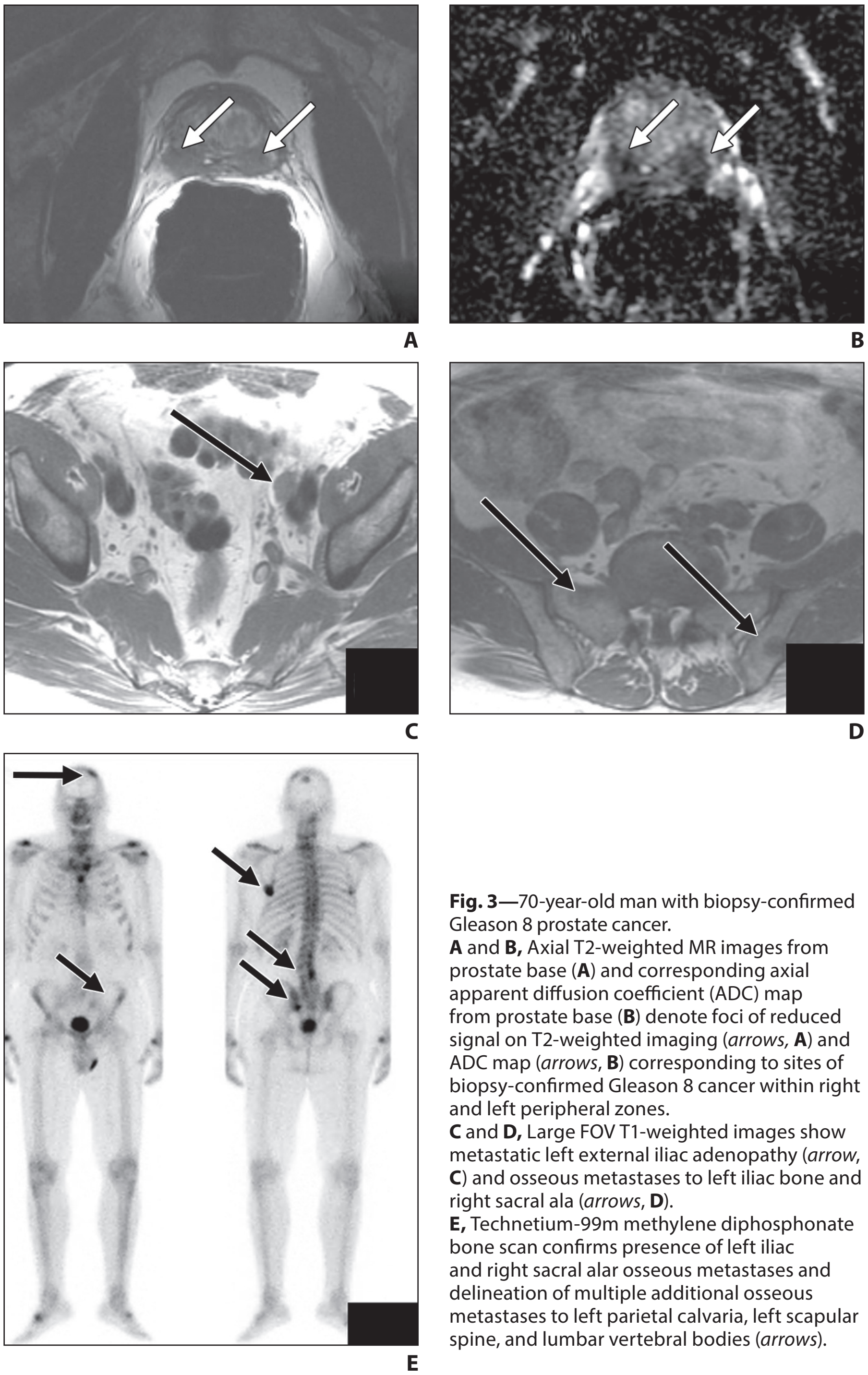

Fig. 3—70-year-old man with biopsy-confirmed Gleason 8 prostate cancer.
A and **B,** Axial T2-weighted MR images from prostate base (**A**) and corresponding axial apparent diffusion coefficient (ADC) map from prostate base (**B**) denote foci of reduced signal on T2-weighted imaging (*arrows*, **A**) and ADC map (*arrows*, **B**) corresponding to sites of biopsy-confirmed Gleason 8 cancer within right and left peripheral zones.
C and **D,** Large FOV T1-weighted images show metastatic left external iliac adenopathy (*arrow*, **C**) and osseous metastases to left iliac bone and right sacral ala (*arrows*, **D**).
E, Technetium-99m methylene diphosphonate bone scan confirms presence of left iliac and right sacral alar osseous metastases and delineation of multiple additional osseous metastases to left parietal calvaria, left scapular spine, and lumbar vertebral bodies (*arrows*).

whole pelvis, large FOV axial T1-weighted images, for example. Common sites for osseous metastatic involvement include the axial and proximal appendicular skeleton, including the pelvic bones and proximal femurs, which may be detectable on whole pelvis, large FOV imaging obtained as part of a prostate MRI or diagnosed on CT of the abdomen and pelvis with administration of IV contrast agent, the latter being an appropriate staging modality in patients with clinically established high-risk prostate cancer [3]. Radionuclide bone scan permits whole-body osseous metastatic involvement and is complementary to MRI or CT for evaluation of possible bone metastases [3] (Fig. 3).

Conclusion

Prostate cancer remains a common malignancy and leading cause of cancer death in men. Radiologic imaging plays an integral role in its diagnosis and staging. Knowledge of prostate anatomy, the indications and imaging findings on US, mpMRI, CT and scintigraphy, staging criteria, and risk stratification metrics enables the practicing radiologist to contribute optimally to patient care.

REFERENCES

1. American Cancer Society website. Key statistics for prostate cancer. www.cancer.org/cancer/prostate-cancer/about/key-statistics.html. Accessed September 1, 2018
2. Epstein JI, Allsbrook W, Amin M, Egevad L, ISUP Grading Committee. The 2005 International Society of Urological Pathology (ISUP) consensus conference on Gleason grading of prostatic carcinoma. *Am J Surg Path* 2005; 29:1228–42
3. Coakley FV, Oto A, Alexander LF, et al. ACR Appropriateness Criteria prostate cancer-pretreatment detection, surveillance, and staging. *J Am Coll Radiol* 2017; 14(5S):S245–S257
4. Lu-Yao GL, Friedman M, Yao SL. Use of radical prostatectomy among Medicare beneficiaries before and after the introduction of prostate specific antigen testing. *J Urol* 1997; 157:2219–22
5. American College of Radiology website. PIRADS v2: prostate imaging—reporting and data system. www.acr.org/-/media/ACR/Files/RADS/Pi-RADS/PIRADS-V2.pdf. Accessed September 1, 2018
6. Padhani AR, Weinreb J, Rosenkrantz AB, Villeirs G, Turkbey B, Barentsz J. Prostate imaging-reporting and data system steering committee. PI-RADS v2 status update and future directions. *Eur Urol* 2018 Jun 13 [Epub ahead of print]
7. American College of Radiology website. PIRADS v2 lexicon. www.acr.org/-/media/ACR/Files/RADS/Pi-RADS/PIRADS-V2-Lexicon.pdf?la=en. Accessed September 1, 2018
8. McNeal JE. The zonal anatomy of the prostate. *Prostate* 1981; 2:35-49
9. Venkatesan AM, Stafford RJ, Duran C, Soni PD, Berlin A, McLaughlin PW. Prostate magnetic resonance imaging for brachytherapists: anatomy and technique. *Brachytherapy* 2017; 16:679–687
10. Hedgire SS, Eberhardt SC, Borczuk R, McDermott S, Harisinghani M. Interpretation and reporting multiparametric prostate MRI: a primer for residents and novices. *Abdom Imaging* 2014; 39:1036–1051
11. McNeal JE, Redwine EA, Freiha FS, et al. Zonal distribution of prostatic adenocarcinoma: correlation with histologic pattern and direction of spread. *Am J Surg Pathol* 1988;12:897–906
12. Welliver C, Helo S, McVary KT. Technique considerations and complication management in transurethral resection of the prostate and photoselective vaporization of the prostate. *Transl Androl Urol* 2017; 6: 695-703
13. Liss A, Zhou J, Evans C, et al. Anatomic variability of the neurovascular elements defined by MRI. *Brachytherapy* 2014; 13:S42–S43
14. NCCN Clinical Practice Guidelines in Oncology. Prostate cancer: version 2.2016. www.nccn.org/professionals/physician_gls/pdf/prostate.pdf. Accessed September 2, 2018
15. Pokorny MR, de Rooij M, Duncan E, et al. Prospective study of diagnostic accuracy comparing prostate cancer detection by transrectal ultrasound-guided biopsy versus magnetic resonance (MR) imaging with subsequent MR-guided biopsy in men without previous prostate biopsies. *Eur Urol* 2014; 66:22–29
16. Turkbey B, Pinto PA, Mani H, et al. Prostate cancer: value of multiparametric MR imaging at 3T for detection-histopathologic correlation. *Radiology* 2010; 255:89–99
17. Hegde JV, Mulkern RV, Panych LP, et al. Multiparametric MRI of prostate cancer: an update on state-of-the art techniques and their performance in detecting and localizing prostate cancer. *J Magn Reson Imaging* 2013; 37:1035–1054
18. Hricak H, White S, Vigneron D, et al. Carcinoma of the prostate gland: MR imaging with pelvic phased-array coils versus integrated endorectal pelvic phased-array coils. *Radiology* 1994;193:703–709
19. Heijmink SW, Futterer JJ, Hambrock T, et al. Prostate cancer: body array versus endorectal coil MR imaging at 3 T—comparison of image quality, localization, and staging performance. *Radiology* 2007; 244:184–195
20. Yakar D, Heijmink SW, Hulsbergen-van de Kaa CA, et al. Initial results of 3-dimensional ^{1}H-magnetic resonance spectroscopic imaging in the localization of prostate cancer at 3 Tesla: should we use an endorectal coil? *Invest Radiol* 2011; 46:301–306
21. Kitajima K, Kaji Y, Fukabori Y, et al. Prostate cancer detection with 3 T MRI: comparison of diffusion-weighted imaging and dynamic contrast-enhanced MRI in combination with T2-weighted imaging. *J Magn Reson Imaging* 2010; 31:625–631
22. Bains LJ, Studer UE, Froehlich JM, et al. Diffusion-weighted magnetic resonance imaging detects significant prostate cancer with high probability. *J Urol* 2014; 192:737–742
23. Rosenkrantz AB, Verma S, Turkbey B. Prostate cancer: top places where tumors hide on multiparametric MRI. *AJR* 2015; 204:[web]W449–W456
24. Hoeks CM, Hambrock T, Yakar D, et al. Transition zone prostate cancer: detection and localization with 3-T multiparametric MR imaging. *Radiology* 2013; 266:207–217
25. Wang L, Mazaheri Y, Zhang J, et al. Assessment of biologic aggressiveness of prostate cancer: correlation of MR signal intensity with Gleason grade after radical prostatectomy. *Radiology* 2008; 246:168–176
26. Barentsz JO, Richenberg J, Clements R, et al. ESUR prostate MR guidelines 2012. *Eur Radiol* 2012; 22:746–757
27. Aydin H, Kizilgoz V, Tatar IG, et al. Detection of prostate cancer with magnetic resonance imaging: optimization of T1- weighted, T2-weighted, dynamic-enhanced T1-weighted, diffusion weighted imaging apparent diffusion coefficient mapping sequences and MR spectroscopy, correlated with biopsy and histopathological findings. *J Comput Assist Tomogr* 2012; 36:30–45
28. Tan CH, Wei W, Johnson V, Kundra V. Diffusion-weighted MRI in the detection of prostate cancer: meta-analysis. *AJR* 2012; 199:822–829
29. Cooperberg MR, Carroll PR, Klotz L. Active surveillance for prostate cancer: progress and promise. *J Clin Oncol* 2011; 29:3669–3676
30. Bae H, Yoshida S, Matsuoka Y, et al. Apparent diffusion coefficient value as a biomarker reflecting morphological and biological features of prostate cancer. *Int Urol Nephrol* 2013; 46:555–561
31. Nagarajan R, Margolis D, Raman S, et al. Correlation of Gleason scores with diffusion-weighted imaging findings of prostatecancer. *Adv Urol* 2012; 2012:374805
32. Yoshizako T, Wada A, Hayashi T, et al. Usefulness of diffusion-weighted imaging and dynamic contrast-enhanced magnetic resonance imaging in the diagnosis of prostate transition-zone cancer. *Acta Radiol*. 2008; 49:1207–1213
33. Verma S, Turkbey B, Muradyan N, et al. Overview of dynamic contrast-enhanced MRI in prostate cancer diagnosis and management. *AJR* 2012; 198:1277–1288
34. Kelloff GJ, Choyke P, Coffey DS, Prostate Cancer Imaging Working Group. Challenges in clinical prostate cancer: role of imaging. *AJR* 2009; 192:1455–1470
35. Cool DW, Zhang X, Romagnoli C, Izawa JI, Romano WM, Fenster A. Evaluation of MRI-TRUS fusion versus cognitive registration accuracy for MRI-targeted, TRUS-guided prostate biopsy. *AJR* 2015; 204:83–91
36. Valerio M, McCartan N, Freeman A, Punwani S, Emberton M, Ahmed HU. Visually directed vs. software-based targeted biopsy compared to transperineal template mapping biopsy in the detection of clinically significant prostate cancer. *Urol Oncol* 2015; 33:424.e9–16
37. Wysock JS, Rosenkrantz AB, Huang WC, et al. A prospective, blinded comparison of magnetic resonance (MR) imaging-ultrasound fusion and visual estimation in the performance of MR-targeted prostate biopsy: the PROFUS trial. *Eur Urol* 2014; 66:343–351
38. Siddiqui MM, Rais-Bahrami S, Turkbey B et al. Comparison of MR/ultrasound fusion-guided biopsy with ultrasound-guided biopsy for the diagnosis of prostate cancer. *JAMA* 2015; 27:390–397
39. Schoots IG, Roobol MJ, Nieboer D, et al. Magnetic resonance imaging-targeted biopsy may enhance the diagnostic accuracy of significant prostate cancer detection compared to standard transrectal ultrasound-guided biopsy: a systematic review and meta-analysis. *Eur Urol* 2015; 68:438–450
40. van de Ven WJ, Barentsz JO. Prostate cancer: MRI/US-guided biopsy—a viable alternative to TRUS-guidance. *Nat Rev Urol* 2013; 10:559–560
41. Klein EA. Prostate cancer: MR-TRUS fusion biopsy—defining a new standard. *Nat Rev Clin Oncol* 2015; 12:253–254
42. Hoeks CM, Schouten MG, Bomers JG, et al. Three-Tesla magnetic resonance-guided prostate biopsy in men with increased prostate specific antigen and repeated, negative, random, systematic, transrectal

ultrasound biopsies: detection of clinically significant prostate cancers. *Eur Urol* 2012; 62:902–909
43. Mendhiratta N, Rosenkrantz AB, Meng X, et al. Magnetic resonance imaging-ultrasound fusion targeted prostate biopsy in a consecutive cohort of men with no previous biopsy: reduction of over detection through improved risk stratification. *J Urol* 2015; 194:1601–1606
44. Hovels AM, Heesakkers RA, Adang EM, et al. The diagnostic accuracy of CT and MRI in the staging of pelvic lymph nodes in patients with prostate cancer: a meta-analysis. *Clin Radiol* 2008; 63:387–395
45. Briganti A, Abdollah F, Nini A, et al. Performance characteristics of computed tomography in detecting lymph node metastases in contemporary patients with prostate cancer treated with extended pelvic lymph node dissection. *Eur Urol* 2012; 61:1132–1138
46. Shen G, Deng H, Hu S, Jia Z. Comparison of choline-PET/CT, MRI, SPECT, and bone scintigraphy in the diagnosis of bone metastases in patients with prostate cancer: a meta-analysis. *Skeletal Radiol* 2014; 43:1503–1513
47. American Joint Committee on Cancer. Prostate. In: *AJCC cancer staging manual*. 8th ed. New York, NY: Springer, 2017: 715-725
48. Buyyounouski MK, Choyke PL, McKenney JK et al. Prostate cancer- major changes in the American Joint Committee on Cancer eighth edition cancer staging manual. *CA Cancer J Clin* 2017; 67:245–253
49. Daneshmand S, Quek ML, Stein JP, et al. Prognosis of patients with lymph node positive prostate cancer following radical prostatectomy: long term results. *J Urol* 2004; 172:2252–2255
50. Fukuda H, Nakagawa T, Shibuya H. Metastases to pelvic lymph nodes from carcinoma in the pelvic cavity: diagnosis using thin-section CT. *Clin Radiol* 1999; 54:237–242
51. Brown G, Richards CJ, Bourne MW, et al. Morphologic predictors of lymph node status in rectal cancer with use of high spatial-resolution MR imaging with histopathologic comparison. *Radiology* 2003; 227:371–377
52. Yang WT, Lam WW, Yu MY, Cheung TH, Metreweli C. Comparison of dynamic helical CT and dynamic MR imaging in the evaluation of pelvic lymph nodes in cervical carcinoma. *AJR* 2000; 175:759–766